Bull. Disas, Prev. Res, Inst., Kyoto Univ., Vol. 26, Part 3, No. 241, Sept., 1976

Erosion and Cross Section on the Cohesive Stream Bed

By Kazuo Ashida and Kenji Sawai

(Manuscript received October 3, 1976)

Abstract

Usually some cohesive materials are contained in bare slopes, where the rill-like streams are formed in the process of surface water erosion. For the prediction of the sediment run-off from such a slope, it is important to know the arrangement and scale of streams and soil property against erosion. In this study a new theoretical model is offered to obtain the shear distribution along the channel perimeter with an arbitrary corss section, and the erosion process of the cohesive material bed is investigated. The theory is examined by flume experiments using bentonite.

Main results are as follows.

The rate of erosion is related to the local shear.

Shear distribution in a uniform flow is obtained by differentiating the area between the normals to the wall with the wetted perimeter.

Bed unevenness in the lateral direction may be amplified or reduced according to the shape of the unevenness and the flow conditions. The criterion is obtained in the domain of a/H and L/H, where a and L are the wave height and length respectively and H is the water depth.

A stream has an equilibrium cross section corresponding to the hydraulic conditions. When the rate of erosion is proportional to the shear velocity, the ratio of the water surface width to the maximum water depth is about 4 in the equilibrium state.

1. Introduction

Usually some cohesive materials are contained in bare slopes, where erosional characteristics distinctly differ from those on the noncohesive bed. For example, the angle of repose is one of the restriction for the shape of the noncohesive bed, but there is not such a restriction for the cohesive bed. Consequently, when the stream position is fixed on the cohesive bed, the bed is locally eroded there, and deep ditches are formed and even overhangs can be seen. Rills often observed on bare slopes are supposed to be the products of such a process.

Another feature of erosion on the cohesive bed is that the sediment supply is less than the transport capacity when the bed length is not sufficiently long, because of the large resistance against detachment. So, flow energy usually acts on the bed as the erosional agent without sediment deposition and the bed level is always lowered.

The study on the erosion of such cohesive beds is not advanced compared with that of noncohesive beds, and the only empirical information under some restricted conditions is used to predict the critical velocity for erosion or sediment run-off. According to the report of ASCE, 1968[1], the previous studies were directed to clarify the erosional resistance of cohesive soils, soil loss from the land, design of the stable channel etc.. But the information about the arrangement and the cross sectional form of the streams on bare slopes, which are necessary to predict the sediment run-off from the hydraulic view points, have not been obtained.

In this study, theoretical and experimental considerations about the transformation process of the channel cross section including rill development are discussed.

2. Rate of erosion of the cohesive material bed

It is known that the rate of erosion of clay has a positive correlation to the tractive force and rapidly varies near the one named critical tractive force, for the fixed condition of clay and water quality etc.. However, the erosion of clay is not only a simple mechanical phenomenon but also an electro-chemical one, so no theoretical approach has been succesful. Some empirical approaches to correlate the critical tractive force to the shear strength of the clay mass, plasticity index, dispersion ratio etc. have been tried[2)3)], but the relation differs from case by case, and it is necessary to do a sample test for each respective soil type.

Partheniades[4)] took up sediment concentration also the parameters relating to erosion and derived the reltaion between tractive force and rate of reosion from probabilistic consideration, but it is not sufficient to be applied generally.

Then, the authors carried out an erosion test of bentonite. The relation between tractive force (τ) and rate of erosion (E) is shown in Fig. 1. The water content and saturation ratio are considered to be indicies representing the condition of bentonite. Fig. 1, corresponding to the fully saturated condition, shows that the rate of erosion of bentonite considerably depends on the water content, and the smaller

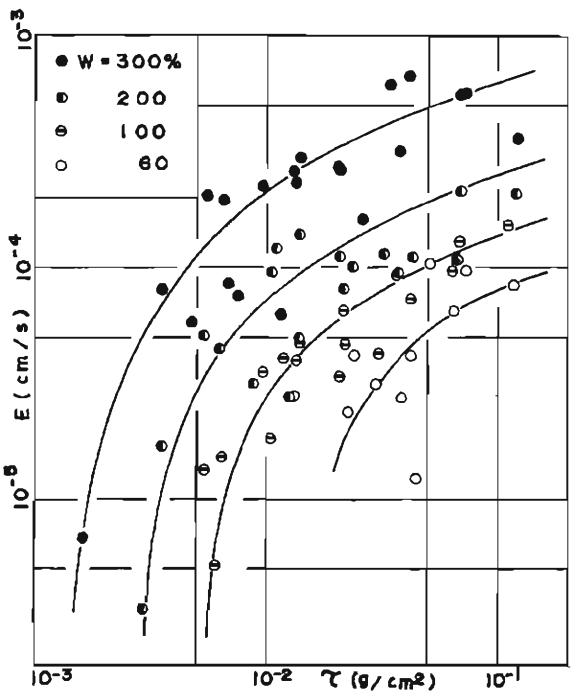

Fig. 1. Rate of erosion related to the tractive force.

the water content, the larger the erosional resistance is. For the fixed water content, the rate of erosion is proportional to the shear velocity in the range of high tractive force.

3. Shear distribution in an arbitrary channel cross section

In a uniform flow, if the effect of the secondary flow is negligible, shear stress does not act on the orthogonal planes to the isovels as shown in Fig. 2(a). So that the gravity component acting in the fluid mass between those orthogonals is balanced

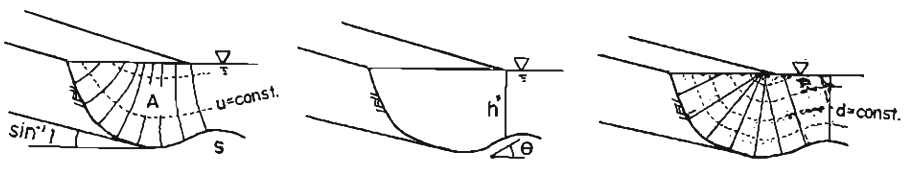

Fig. 2. Various calculation methods of tractive force.
(a) With orthogonals of isovels.
(b) With vetricals (h': Local water depth, θ: Wall inclination).
(c) With orthogonals of equi-distance lines from the wall.

with only the shear along the wetted perimeter so-called tractive force. Consequently, the tractive force τ is represented as follows,

$$\tau = \rho g(dA/ds)I \qquad \cdots\cdots(1)$$

where, A is the area between orthogonals, s is the wetted perimeter, ρ is the fluid density, g is the acceleration of gravity and I is the longitudinal channel slope.

It is very difficult to obtain isolves in an arbitrary channel cross section, so that the orthogonals are usually replaced with the verticals as shown in Fig. 2(b). Then, the shear distribution is approximated by the next equation.

$$\tau = \rho g h' I \cos\theta \qquad \cdots\cdots(2)$$

where, h' is the local water depth and θ is the inclination of the wall. This approximation is, however, unreasonable, not only because the shear acting on the vertical side wall can not be evaluated but also because the shear at the deep is maximum regardless of the curvature. Thus, the authors propose to replace isovels with equi-distance lines from the wall as shown in Fig. 2(c), by which it becomes possible to obtain the shear distribution graphically, and to represent the sheltering effect at the concaves and the shear concentration at the convexes. For the orthogonals coincide with the normal lines to the wall, Eq. (1) reduces to the following form, as long as those normal lines do not cross one another. Using the symbols shown in Fig. 3, the equation is,

$$\frac{\tau}{\rho ghI} = \frac{dA/ds}{h} = \frac{1}{h}\frac{dx}{ds}\frac{d}{dx}\left[\int_0^x \{y_n(\zeta)-y(\zeta)\}d\zeta - A'\right]$$

$$= \frac{1}{h}\frac{dx}{ds}\frac{d}{dx}\left[\int_0^x \left\{y(x)+\frac{dx}{dy}(x-\zeta)-y(\zeta)\right\}d\zeta - \frac{1}{2}\left\{\max\left[0,\ x-(h-y(x))\frac{dy}{dx}\right]\right\}^2\frac{dx}{dy}\right]$$

$$= \frac{\left\{1+(dY/dX)^2-\frac{1}{2}(d^2Y/dX^2)\cdot F\right\}\cdot F}{\sqrt{1+(dY/dX)^2}}, \quad F = \min\left[1-Y,\ X\frac{dX}{dY}\right] \qquad \cdots\cdots\cdots(3)$$

Where, h is the maximum water depth, X and Y are the coordinates of the wall normalized with h. One of the distinctive features of this equation is that the curvature of the wall is introduced by the existence of the second order derivative d^2Y/dX^2. When both of dY/dX and d^2Y/dX^2 are small, this equation coincides with Eq. (2).

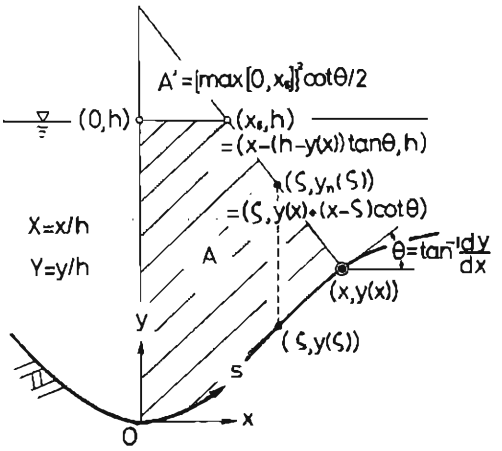

Fig. 3. Definition sketch for Eq. (3).

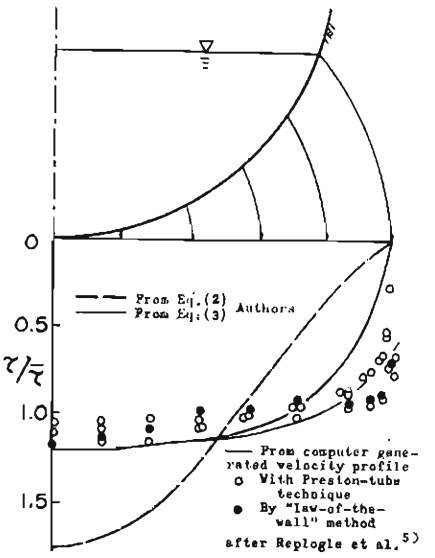

Fig. 4. Various determinations of shear stress distribution in a circular channel.

Fig. 4 shows the shear stress distributions determined from various methods, in a circular channel with width-depth ratio 3. Eq. (3) is much better than Eq. (2), though the mean tractive force coincides in both equations, i.e.

$$\bar{\tau} = \frac{1}{P}\int_0^P \rho g\frac{dA}{ds}Ids = \frac{1}{P}\int_0^B \rho gh'I\cos\theta ds = \frac{\rho gAI}{P} = \rho gRI \qquad \cdots\cdots\cdots(4)$$

where, P is the wetted perimeter, B is the water surface width and R is the hydraulic radius.

4. Amplification and reduction of the lateral bed unevenness

Generally, there are various scales in the lateral unevenness on the slope or on the channel bed. When the rate of erosion at the trough is larger than that at the ridge, the unevenness grows, and in the case of the contrary the unevenness reduces. Therefore it is important to compare the rates of erosion at the trough and ridge of the unevenness.

4.1 Theoretical approach

For the convenience of the analysis, the form of the unevenness is assumed to be approximately represented by a single sine-wave shown in Fig. 5, i.e.

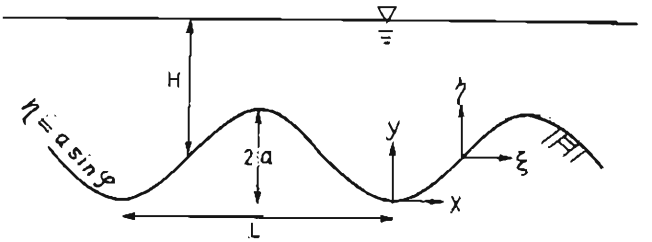

Fig. 5. Definition sketch for Eq. (5).

$$\eta = a \sin (2\pi\xi/L) \qquad \cdots\cdots(5),$$

where, a is the amplitude, L is the wave length and $(\xi, \eta)=(x-L/4, y-a)$. Then the shear distribution becomes from Eq. (3),

$$\frac{\tau}{\rho gHI} = \frac{\{1+\delta^2\cos^2\varphi+(\delta^2/2\alpha)\sin\varphi\cdot F'\}\cdot F'}{\sqrt{1+\delta^2\cos^2\varphi}}, \quad F' = \min\left[1-\alpha\sin\varphi, \frac{\alpha(2\varphi+\pi)}{2\delta^2\cos\varphi}\right] \qquad \cdots\cdots(6)$$

and the mean shear value derives from Eq. (4),

$$\frac{\bar{\tau}}{\rho gHI} = \frac{A}{HP} = \int_{-L/4}^{L/4}(H-\eta)\,d\xi \Big/ H\int_{-L/4}^{L/4}\sqrt{1+\left(\frac{d\eta}{d\xi}\right)^2}\,d\xi = \frac{\pi}{2\sqrt{1+\delta^2 E(\sin(\tan^{-1}\delta))}}, \qquad \cdots\cdots(7),$$

where, $\alpha=a/H$, $\delta=2\pi a/L$, $H=h-a$, $\varphi=2\pi\xi/L$ and $\mathrm{E}(\sin(\tan^{-1}\delta))=\int_0^{\pi/2}\sqrt{1-\sin^2(\tan^{-1}\delta)\sin^2\varphi}\,d\varphi$. Then the ratio of the local shear stress to the mean one becomes,

$$\frac{\tau}{\bar{\tau}} = \frac{2}{\pi}\mathrm{E}(\sin(\tan^{-1}\delta))\sqrt{\frac{1+\delta^2}{1+\delta^2\cos^2\varphi}}\left\{1+\delta^2\cos^2\varphi+\frac{\delta^2}{2\alpha}\sin\varphi\cdot F'\right\}\cdot F' \qquad \cdots\cdots(8).$$

Fig. 6 shows the shear stress distribution obtained from Eq. (8) on the furrow-like stream bed with various wave lengths and heights.

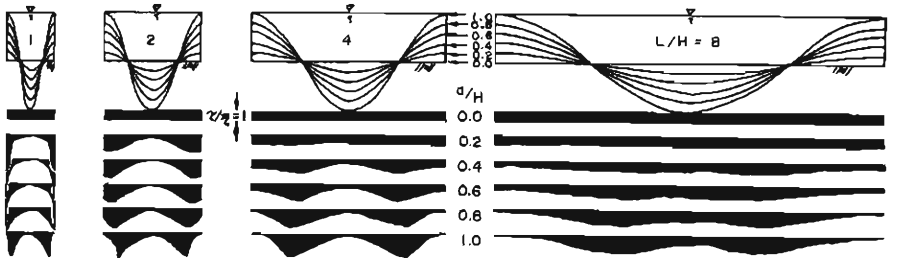

Fig. 6. Shear stress distribution on the furrow-like stream bed.

By the way, the rate of erosion correlates positively to the shear. So, when the shear at the trough is larger than at the ridge, the unevenness amplifies, and when the shear at the ridge is larger than at the trough, the unevenness reduces. The shears at the ridge and at the trough are obtained from Eq. (8) by replacing φ with $\pm\pi/2$, i.e.

$$\tau_{\text{ridge}}/\rho gHI = \left\{1+\frac{1}{2}K\alpha(1-\alpha)\right\}(1-\alpha) \qquad \cdots\cdots(9)$$

$$\tau_{\text{trough}}/\rho gHI = \begin{cases} 1/(2K\alpha) & [(2\alpha+1)^2 \geqq 1+(4/K)] \\ \left\{1-\frac{1}{2}K\alpha(1+\alpha)\right\}(1+\alpha) & [(2\alpha+1)^2 \leqq 1+(4/K)] \end{cases} \qquad \cdots\cdots(10)$$

where, $K \equiv (\delta/\alpha)^2 = (2\pi H/L)^2$.

Fig. 7 shows the stability diagram derived from Eq. (9) and Eq. (10). The unevenness grows in the region indicated by the upward arrows, reduces in the region indicated by the downward arrows, and is in equilibrium on the boundary between them and on the axis of the abscissas. If the form of the unevenness remains sinusoidal and the wave length and water depth do not change in the process of erosion, any point on Fig. 7 moves to the direction indicated by the arrow there, i.e. the

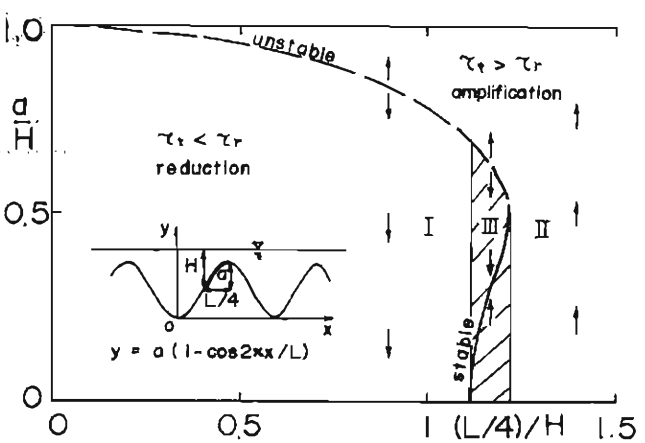

Fig. 7. Stability diagram of the furrow-like stream bed.

unevenness reduces to zero in region I; grows to split itself in region II; and approaches to the equilibrium state in region III. Though both the solid and broken lines in Fig. 7 indicate equilibrium states, the former indicates the stable equilibrium state in the sense that the deviation from it diminishes and the latter indicates the unstable equilibrium state in the sense that the point near it goes away toward another state.

Putting the depth from a datum line to the ridge of the bed z_r, and that to the trough z_t as shown in Fig. 8, the amplitude of the unevenness is,

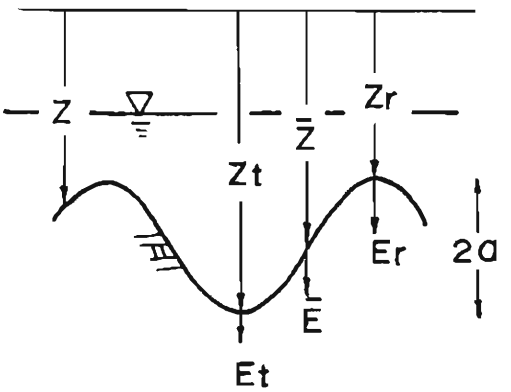

Fig. 8. Definition sketch for Eq. (11).

$$a = (z_t - z_r)/2 \qquad \cdots\cdots(11)$$

whose rate of change is,

$$da/dt = (E_t - E_r)/2 \fallingdotseq \frac{1}{2}(dE/du_*) \cdot \Delta u_* \qquad \cdots\cdots(12)$$

where, $E_r = dz_r/dt$, $E_t = dz_t/dt$, $\Delta u_* = u_{*t} - u_{*r}$, u_{*r} and u_{*t} represent the shear velocity at the ridge and at the trough respectively.

When the relation between shear velocity and rate of erosion is represented as

$$E \propto u_*^n \qquad \cdots\cdots(13),$$

Eq. (12) becomes

$$(da/dt)/E_0 \fallingdotseq (n/2) \cdot (\Delta u_*/U_*) \qquad \cdots\cdots(14),$$

where n is the constant concerned with soil nature and shear range, E_0 is the rate of erosion corresponding to U_* and $U_* = \sqrt{gHI}$.

As mentioned above, n is nearly equal to unity in the range of high tractive force in the case of bentonite.

Substituting Eqs. (9), (10) into Δu_* in Eq. (14), and putting $n=1$, the diagram of amplification rate is obtained as shown in Fig. 9. In Fig. 9 upward arrows represent amplification and downward arrows represent reduction of unevenness, and the

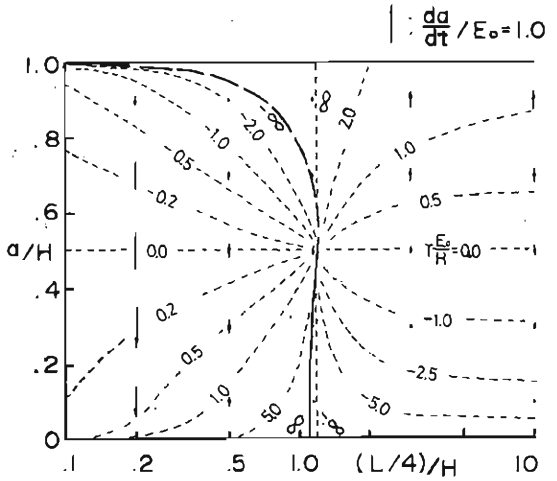

Fig. 9. Amplification rate and the time required.

length of arrows are proportional to the rate of those amplification or reduction i.e. values of Eq. (14).

Integrating the reciprocal of the amplification rate, the time required for the change of the amplitude is obtained. Putting the initial point of integration at the state where the amplitude is half of the mean depth, the time T is,

$$\frac{T}{H/E_0} = \frac{E_0}{H}\int_{H/2}^{a} \frac{dt}{da}\,da \fallingdotseq \int_{1/2}^{a/H} \frac{2U_*}{n\Delta u_*}\,d\left(\frac{a}{H}\right) \qquad \cdots\cdots(15).$$

The numerals on the dotted lines in Fig. 9 show the values of Eq. (15) in the case of $n=1$ and mean depth H being time-independent.

As shown in Fig. 9, the rate of amplification or reduction is small near the boundary between the two regions and in the range of small amplitude. For the constant furrow intervals L, there is a certain wave height in which the reduction rate ($|da/dt|$) is maximum in the region of reduction, but the higher the wave height is, the faster it grows in the region of amplification. For the constant wave height, the unevenness with narrower intervals is easy to reduce, and that with wider intervals is easy to amplify.

On the other hand, the average bed level lowers in the process of erosion. For the sinusoidal stream bed, the average bed is equal to the middle of the ridge and trough, so the depth from the datum line to the average bed level $\bar{z}$ as shown in Fig. 8 is,

$$\bar{z} = (z_t + z_r)/2 \qquad \cdots\cdots(16),$$

and the lowering rate $\bar{E}$ is,

$$\bar{E} = d\bar{z}/dt = (E_r + E_t)/2 \fallingdotseq E_{(\bar{u}_*)} \qquad \cdots\cdots(17),$$

where $E_{(\bar{u}_*)}$ is the rate of erosion corresponding to the mean shear velocity

$u_*[=(u_{*l}+u_{*r})/2]$. Normalizing with E_0 and using Eq. (13), E.q (17) becomes,

$$\bar{E}/E_0 \fallingdotseq (u_*/U_*)^n \qquad \cdots\cdots(18).$$

Further, the average lowering height Z from the state in which the amplitude is half of the depth H is,

$$\frac{Z}{H} = \frac{1}{H}\int_{H/2}^{a} \frac{d\bar{z}}{da}\,da = \frac{1}{H}\int_{H/2}^{a} \frac{\bar{E}}{da/dt}\,da = \int_{1/2}^{a/H} \frac{2}{n}\cdot\left(\frac{u_*}{U_*}\right)^{n-1} \frac{u_*}{\Delta u_*}\,d\left(\frac{a}{H}\right) \qquad \cdots\cdots(19).$$

In Fig. 10, arrows represent the scouring rate in Eq. (18) and the numerals on the dotted lines represent the scouring depth in Eq. (19), using Eqs. (9), (10) and putting $n=1$.

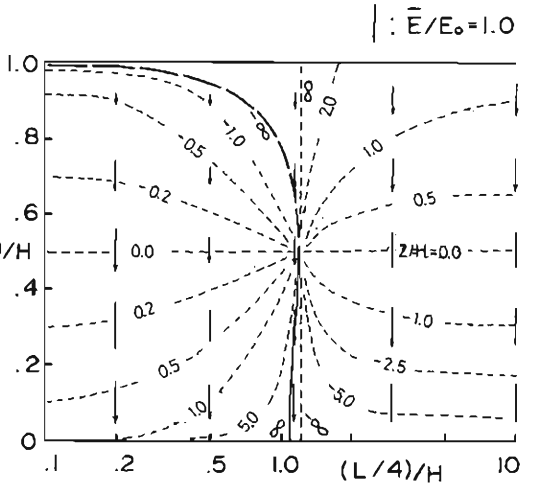

Fig. 10. Average scouring rate and the scouring depth.

Some of the unevennesses of the stream bed among various scales grow to split its water surface, which is supposed to be the mechanism of rill generation on the bare slopes. By the way, the width of stream is not practically infinite, so the scale of the lateral unevenness is restricted as follows,

$$L/B<1/2 \qquad \cdots\cdots(20)$$

where, L is the wave length (furrow interval) of the lateral bed unevenness and B is the water surface width of stream. As sohwn in Fig. 9, when the amplitude is infinitely small, the bed is stable, neutral or unstable for each of the next three conditions respectively,

$$(L/4)/H \lessgtr \sqrt{2}\,\pi/4 \fallingdotseq 1.1 \qquad \cdots\cdots(21).$$

Among the unevennesses satisfying the unstable condition, those which grow to split their water surface must moreover satisfy the next condition,

$$(L/4)/H > \pi/4\sqrt{\sqrt{2}-1} \fallingdotseq 1.2 \qquad \cdots\cdots(22).$$

Therefore, the condition under which such unevennesses can exist is from Eqs. (20) and (22),

$$B/H > 2\pi/\sqrt{\sqrt{2}-1} \fallingdotseq 10 \qquad \cdots\cdots\cdots\cdots\cdots\cdots(23).$$

As far as the stream satisfies this condition, it will be split into more parts in succession. But the pattern of the split depends on the initial distribution of the wave length or height, and is not necessarily unique for the given hydraulic or soil condition. The time required for the split also depends on the initial condition, and rapidly increases when the initial height is small, as shown in Fig. 9.

In the foregoing argument, although the unevenness may be composed of various different scales, the amplification and reduction model derived from the single sinusoidal wave was applied, so that more consideration will be necessary, for example, about the phase effect in the superposition.

4.2 Experimental approach

To examine the foregoing theoretical results, some experiments were carried out (Series A). As the bed material, the mixture of sand, bentonite and water with the ratio of 9:1:3 in weight was used. Sand diameter was 1 mm or 0.3 mm and nearly uniform. So, the pores of the sand were nearly filled with the saturated bentonite whose water content is about 300%. The mixture was set in the inclined flume with furrow-like wavy surface and the water was supplied from the upper-end of the flume. The level of the water surface and the bed form were measured

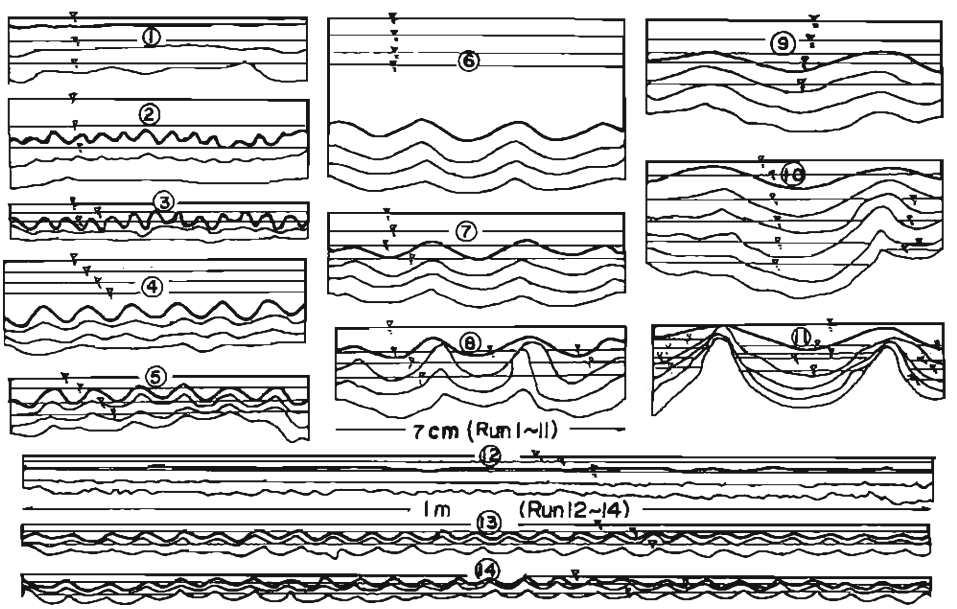

Fig. 11. Growing and attenuating process of the furrow-like stream bed (Exp. Series A).

Table 1. Experimental conditions and results (Series A).

	Run 1	Run 2	Run 3	Run 4	Run 5	Run 6	Run 7	Run 8	Run 9	Run 10	Run 11	Run 12	Run 13	Run 14
Q (l/s)	0.1	0.6	0.15	0.6	0.15	1.2	0.6	0.15	0.6	0.3	0.15	6.6	6.6	4.3
I	1/5	1/20	3/10	1/20	3/10	1/40	1/20	3/10	1/20	1/5	3/10	1/20	1/20	1/20
H (cm)	0.17	0.85	0.35	1.1	0.4	2.5	0.8	0.45	0.9	0.4	0.3	1.5	1.0	0.8
L (cm)	7	0.5		1		2			4			100	4	
a (cm)	0.25												0.50	
t (min) a (cm)	10 0.05	5 0.04	5 0.04	10 0.15	5 0.15	5 0.25	5 0.23	5 $>H$	5 0.25	5 0.38	5 $>H$	16 0.10	16 0.60	48 0.45
t (min) a (cm)	20 0.07	10 0.04	10 0.04	20 0.10	10 0.07	10 0.22	10 0.20		10 0.25			45 0.15	45 0.45	
t (min) a (cm)				30 0.10	15 0.07	15 0.18	15 0.19	15 0.15	15 0.25			75 0.40		
t (min) B/h								5 2.82		15 3.73	15 3.37			48 3.41

with time, and are shown in Fig. 11. Experimental conditions and results are summarized in Table 1.

The outline of Exp. Series A is qualitatively described as follows:

When the intervals of furrows are narrow as in Run 2—Run 5, the bed is eroded much faster at the ridge than at the trough, and the wave height rapidly reduces. On the other hand, when the intervals are wide and the water depth is comparable with the wave height, as Run 11, the bed is eroded faster at the trough than at the ridge, and the wave height grows until the stream splits into parts. When the intervals are medium as Run 6—Run 9, the bed changes into the form with sharp ridges, but thereafter it lowered holding a nearly constant form.

These features are explained from the shear distribution already shown in Fig. 6.

In Fig. 12, the process of Exp. Series A are traced on the plane of Fig. 7, which shows the theory can be applied to some extent quantitavely, too. Numerals in the figure indicate the time normalized by the mean water depth and the mean lowering rate of the bed.

The trace of Run 8 is complicated, in that the wave height grows to split its water surface immediately after the initiation of the water supply, thereafter the split parts join together again to reduce the wave height. This process is understood as follows: In the early state, the rate of erosion was larger at the trough than at the ridge, the level of the water surface lowered faster than the level of the ridge, which became exposed above the flow, but the individual split stream parts were too deep and narrow compared with the equilibrium form corresponding to the hydraulic conditions. So they were widend to scour the foot of their partition walls. Then, the overhung partitions were destroyed for the streams to be joined together. There-

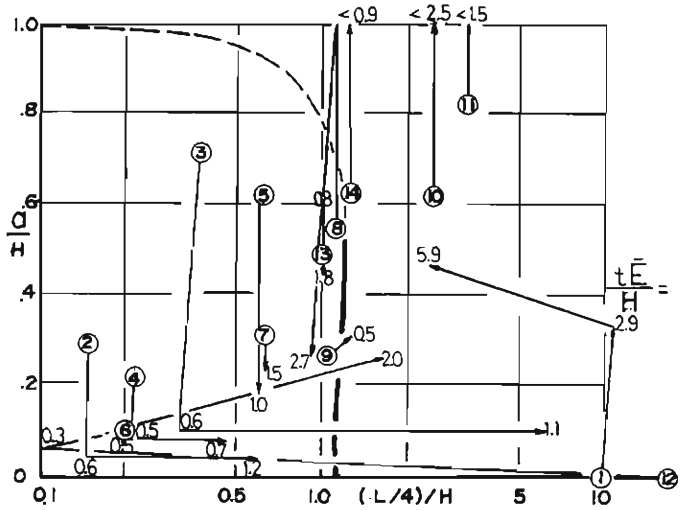

Fig. 12. Trace of Exp. Series A on the wave length-amplitude plane.

fore, it is supposed that the shear at the ridge came to be larger than at the trough, as Run 2—Run 5 and Run 13.

On the other hand, in Run 11 and partly in Run 14, after the unevenness had grown to split into parts in the early stage, the individual split parts lowered keeping approximately constant forms. In this case it is supposed that because the individual stream may be flatter than the equilibrium form at the moment of split, it approaches to the equilibrium state, being eroded at the center to reduce the width. If the split streams join together again, it may be not by the widening but by the meandering of them.

Run 10 is the medium one between Run 8 and Run 11, 14.

It is not because of the change of wave length (L), but because of the change of water depth (H) i.e. because of the change of the flow resistance accompanied with erosion, that the abscissa of this figure slightly shifts as Run 9. It is the result of selective survival of the large wave length, that the abscissa largely shifts to the right as Run 2, 3, 4 and lately in Run 12. And it is because of the generation of new unevenness with smaller scales than the flume width on the initial flat bed whose wave length is regarded to be the flume width, that the abscissa largely shifts to the left as Run 1 and the early stage of Run 12.

Thus, in the actual erosion phenomena, there are various scales of unevenness and the prevailing wave length is not necessarily constant with time.

In this experiment, the condition such as Eq. (23) in which rills generate from a flat bed could not be confirmed. When the amplitude is small, the rate of growth is also so small, that experiments over a long time would be required to confirm it.

5. Formation of the equilibrium channel cross section

5.1 Transformation of the channel cross section

As mentioned before, the wall surface of a cohesive stream bed is eroded corresponding to the respective local shear, and unless a kind of special condition is satisfied, the cross section is generally transformed in the process of erosion. Then it is necessary to know the shear distribution in the cross section and the relation between the shear and the rate of erosion, in order to follow the process hydraulically. When the shear distribution is given by Eq. (1) replacing the isovels approximately with the equidistance lines, and the retiring rate normal to the wall surface is related to the shear velocity using Eq. (13), the transformation of the cross section can be analized graphically. The law of resistance is necessary to determine the water depth from the given discharge and inclination, for the water depth must generally change in the process of erosion.

Here, we have several interesting problems; Is the equilibrium cross section always formed from an arbitrary initial one? What is the shape of equilibrium cross section like and does it depend on the initial condition?

In Fig. 13, the transforming process of the cross sections with parabolic initial forms is traced by a method of numerical finite differences. The shear distribution was calculated from Eq. (3), and for the ratio of the rate of erosion to the shear velocity and the coefficient of flow resistance f, the numerals shown in the figure were used to compare with the experiment described later.

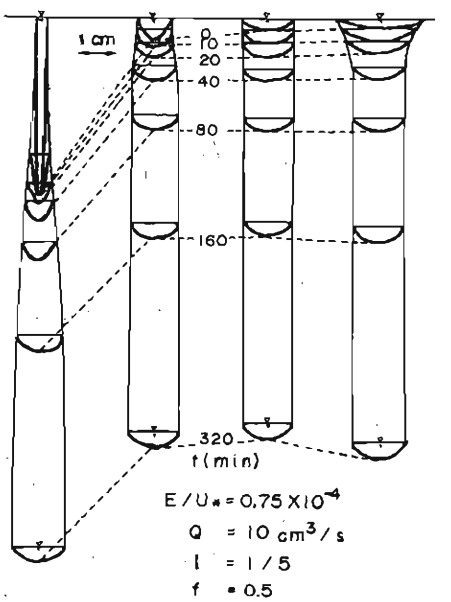

Fig. 13. Transformation process of channel cross section (simulated by method of numerical finite differences).

As shown in Fig. 13, when the initial cross section is narrow and deep, the width widens and the depth reduces. On the other hand, when the initial cross section is wide and shallow, deepening occurs and the width reduces. In this way, though the rates of transformation are different, the cross sections approach to the nearly equal equilibrium forms.

But the uniqueness of the equilibrium state found there is no more than that derived from smooth parabolic initial forms. From the wavy initial forms belonging to the amplification region mentioned above, it is supposed that after the stream is split into parts, they form their own equilibrium cross sections. The pattern of split will depend on the distribution of the wave length and wave height and the composition of the phase in the initial state.

The actual surface of the slope is irregular even just after the work, and not only in the initial form but also in the process of erosion, there are various irregular phenomena. Therefore, in order to deal with the stream forming process generally, it will be necessary to introduce the statistical approach along with the deterministic one.

5.2 Equilibrium channel cross section

In the previous section, the existence of the equilibrium channel cross section was clarified. In this section, the authors derive the equation to determine the equilibrium cross section and obtain the form of the cross section by solving the equation numerically, and examine it through experiments.

The condition that the stream lowers while keeping the same cross section is,

$$\partial z/\partial t = E/\cos\theta = \text{const.} \qquad \cdots\cdots(24).$$

Substituting Eq. (13) and Eq. (3), Eq. (24) reduces to,

$$C = \left\{1+\left(\frac{dY}{dX}\right)^2 - \frac{1}{2}\frac{d^2Y}{dX^2}\cdot F\right\}\cdot F\cdot\left\{1+\left(\frac{dY}{dX}\right)^2\right\}^{1/n-1/2}, \quad F = \min\left[1-Y,\ X\frac{dX}{dY}\right] \qquad \cdots\cdots(25)$$

where C is the ratio of the tractive force to ρghI at the point of maximum depth. Fig. 14 shows the integration of Eq. (25) under the condition of $Y=0$, $dY/dX=0$ at $X=0$ and $n=1$.

When $C<0.833$, the solution rises vertically in the water, and the normals to the wall are entangled with one another. On the other hand, when $C>0.833$, the maximum bed level appears at $X\fallingdotseq 2$, and the transverse wavy bed is obtained with the ratio of the furrow interval to the maximum water depth by about 4. But in that case, for the waterside does not appear, and the width of the stream is infinitely large, it cannot be the solution for the actual one with finite scales. Only when $C\fallingdotseq 0.833$, does the ridge coincide with the water surface, and the closed equilibrium cross section with the ratio of the water surface width to the maximum depth by 4 is obtained.

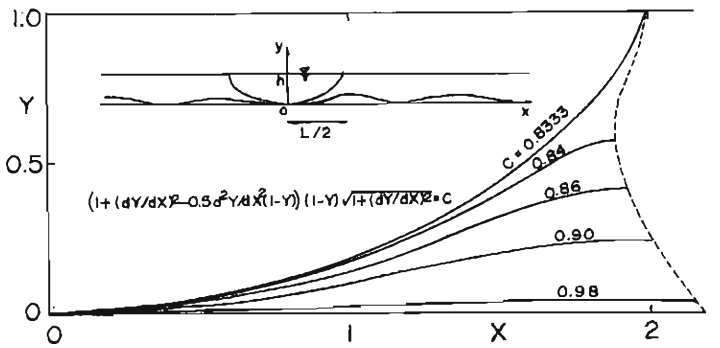

Fig. 14. Theoretical equilibrium channel cross sections.

Thus the equilibrium channel cross sections obtained from this model are similar independent of the hydraulic parameters such as discharge or inclination of the streams. This result comes from the proportionality between the shear and the rate of erosion, thus the form of the cross section would change by considering the critical shear or the exponent n in Eq. (13).

Table 2 and Fig. 15 show the conditions and results of the experiment (Series B) carried out for the formation of the equilibrium channel cross section with cohesive bed material. The material in Run 1—9 is the mixture of sand and bentonite as in the above mentioned Exp. Series A, and that in Run 10 is the soil taken at the Rakusai New Town in Kyoto, Japan. Initial cross sections had been cut rectangulaly, with the width of 1 cm.

Table 2. Experimental conditions and results (Series B).

	Run 1	Run 2	Run 3	Run 4	Run 5	Run 6	Run 7	Run 8	Run 9	Run 10
Q (cm³/s)	5	9	20	2	5	10	1	2	5	10
$\sin^{-1} I$	13°			26°			45°			33°
t (min)	180	180	120	210	120	90	18	105	75	20
B (cm)	1.33	1.20	2.20	0.90	1.26	1.68		0.83	1.20	1.25
h (cm)	0.32	0.32	0.63	0.27	0.34	0.36		0.21	0.35	0.39

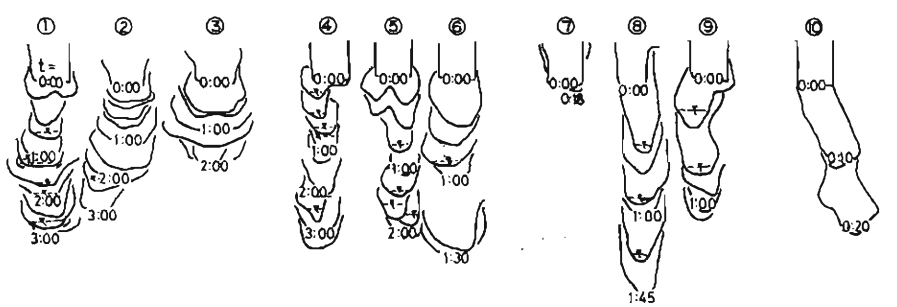

Fig. 15. Transformation process of channel cross section (Exp. Series B).

In a short time after the water supply, they were transformed into the parabolic forms. Thereafter, though the longitudinal bed forms get to have steps and the lateral stream positions considerably deviate, the forms of the cross section are adjusted faster into the equilibrium forms. Therefore, they do not change considerably through the experiment, but for Run 1 and Run 5. (In Run 1, 5, the streams once split, joined again upstream from the measuring point because of meander.)

Though the scales of the cross sections depend on the hydraulic parameters such as discharge or inclination, it is difficult to determine the systematic differences in their forms, whose ratio of the water surface width to the maximum water depth lies in the range from 3 to 4. This value is close to the theoretical one i.e. $B/h \fallingdotseq 4$.

It seems to be by the lateral stream migration or the crash of the side wall, that the channel width at the upper part is wider than at the water surface.

Comparing the nearly constant forms found after the early change in Run 6—9 of Exp. Series A with the theoretical wavy equilibrium forms, some of the experimental ones have a much smaller ratio of the wave length to the water depth and have sharper ridges. Although it is difficult to judge whether they are actual equilibrium forms or they are transient ones transforming toward the equilibrium ones very slowly, as far as the shear distribution is calculated by Eq. (3), the sharpness of the ridge cannot be explained. Then it will be necessary to consider the effect of the secondary flow[6].

By the way, when the form of the channel cross section is obtained, its scale such as depth or width is related to the composition of discharge and inclination by giving a law of flow resistance. But there are many unknown factors concerning the resistance of the flow in slope erosion, for example, the effect of the form of cross section, meander, longitudinal steps of the bed etc.. It is a problem to be clarified in future.

6. Conclusions

For the prediction of the sediment run-off from bare slopes, the process of rill formation on the flat slope, and its transformation toward the equilibrium channel cross section was considered theoretically. The applicability of the theory was examined through some experiments.

The results obtained are summarized as follows.

1) The rate of erosion of cohesive materials depends not only on the flow condition but also on the composition and existing condition of soil. When the other conditions are kept constant, the rate of erosion correlates positively to the tractive force. According to our experiment in the case of bentonite, the correlation is linear in high shear range.

2) Shear distribution along the perimeter in the cross section of uniform flow is obtained by differentiating the area between the orthogonal lines to the isovels with the wetted perimeter. For simplification, the authors proposed to replace the isovels with the equi-distance lines from the perimeter and derived the equation of shear distribution in the arbitrary channel cross section, in which the curvature of

the wall surface is contained and it is quantitatively represented that the shear increases at the convexes and decreases at the concaves.

3) Using the shear distribution and the nature of erosion, it is possible to trace the transforming process of the arbitrary channel cross sections. Representing the lateral bed unevenness in a sinusoidal wave, it was derived that the unevenness with the extremely short wave length is smoothed out in the process of erosion, and that with large wave length compared with the water depth ($L/H \gtrsim 5$) develops to split the water surface into parts.

4) Applying this model to the parabolic cross section, the following processes were traced: The cross section whose initial form is wide and shallow is deepened at a portion of the bed and that whose initial form is narrow and deep is widened toward the nearly equal equilibrium cross sections. When the rate of erosion is proportional to the shear velocity, these equilibrium cross sections are similar irrespective of discharge or inclination of the stream, with the ratio of water surface width to the maximum water depth of about 4.

5) When the form of the channel cross section is obtained, its scale is related to the composition of discharge and inclination by giving a law of flow resistance, which is in turn related to the longitudinal, cross-sectional and plane geometry of the channel and cannot be generally grasped.

Further, although the effect of the secondary flow was neglected in this research, regarding the flow as nearly uniform, the actual flow is often so complicated that the calculating method of shear distribution has to be improved.

6) In this paper the authors argued the formation process of the channel cross section mainly from deterministic viewpoints. In the actual phenomena, however, the existence of the irregularity is inevitable not only in hydrological, geomorphological or soil mechanical conditions but also in the hydraulic mechanism of the flow itself. Therefore it will be necessary to join both the deterministic and statistical approaches together for these problems.

References

1) Task committee on Erosion of Cohesive Materials: Erosion of cohesive sediments, Proc. of ASCE, Vol. 94, No. HY. 4, 1968.
2) Dunn, Irving S.: Tractive resistance of cohesive channels, Proc. of ASCE, Vol. 85, No. SM3, 1959.
3) Smerdon, E.T., and Beasley, R.P.: Tractive force theory applied to stability of open channels in cohesive soils, Research Bulletin No. 715, Agricultural Experiment Station, Univ. of Missouri, Columbia, Mo., 1959.
4) Partheniades, E.: Erosion and Deposition of Cohesive Materials, River Mechanics, vol. II ed. by H.W. Shen, 1971.
5) Graf, W.H.: Hydraulics of Sediment Transport, McGraw-Hill, 1971, p. 112.
6) Allen, J.R.L.: Transverse erosional marks of mud and rock: Their physical basis and geological significance, Sediment Geol., 5, 1971, p. 320.